SFST: a robust framework for heart rate monitoring from photoplethysmography signals during physical activities

Zhao, Teddy; Sun, Yu; Wan, Suiren; Wang, Feng

SFST: a Robust Framework for Heart Rate Monitoring from Photoplethysmography Signals during Physical Activities

Teddy Zhao[a,b], Suiren Wan[a], Yu Sun[c], Feng Wang[a]

[a]*Biological Science and Medical Engineering, Southeast University, Nanjing, China*
[b]*LTSI, Université de Rennes 1, Rennes, France*
[c]*Cancer and Genomic Science, University of Birmingham, Birmingham, England*

Abstract

As a non-invasive approach to monitor heart rate (HR), the photoplethysmography (PPG) signal provides a simple and accurate measurement in silence. However, difficulties are found when dealing with signals monitored during physical activities, because complex noise shares a very close frequency bin with HR. Traditional analogue filters can hardly derive HR in this situation. This paper is aimed to establish a joint framework for HR monitoring from PPG signals during physical activities. A combination of Short-time Fourier Transform (STFT) and spectral analysis was adopted as the principal part, with a medium filter as assisted. The time-frequency resolution in low frequency is enhanced by the size-fixed window function in STFT. Based on 12 datasets sampled at 25 Hz and recorded during different physical activities, the HR data derived via the proposed algorithm was analysed. The average absolute estimation error was 1.06 beats/min and the standard deviation was 0.69 beats/min. Compared with the true HR via ECG, the cross-correlation average was 0.9917 beats/min and the standard deviation was 0.0141 beats/min. Therefore, the proposed framework is proved reliable for HR monitoring from PPG during physical activities of high intensity. It can be applied to smart wearable devices for fitness tracking and health information tracking.

Keywords: PPG, STFT, heart rate monitoring, spectral analysis

1. Introduction

Heart rate (HR) can be observed using the photoplethysmography (PPG) signal via the electrical equipment [1]. It is widely used for wearable devices in research and development [2]. Compared with the electrocardiogram (ECG) signals, the PPG signal gets rid of the complex hardware implementation and the requirement of the reference signal [3]. At the beginning, analogue filtering techniques are suggested to process PPG signals monitored at rest [4]. However, motion artefacts (MA) and HR share a very close frequency bin in physical activities, resulting in extreme difficulties for HR estimation. To address this issue, most proposed algorithms are dealing with the time domain. Yet they are not so effective to enhance the accuracy, nor feasible for signals detected during high-intensity physical activities.

One of the popular methods is the adaptive noise cancelation (ANC) [5]. It is demonstrated reliable for electroencephalography (EEG) signals [6]. The acceleration signal provided by the micro-electro-mechanical system (MEMS) reflects MA in a certain extent. It is then used as the reference signal in the adaptive filter [7]. At the same time, the performance of ANC is sensitive to the reference signal [8]. Some other adaptive algorithms such as adaptive least mean square (LMS) [9], adaptive comb filters [10], adaptive step-size least mean squares (AS-LMS) [11], two-stage normalised least mean square adaptive noise canceler [12] are then proposed. On the other hand, the independent components analysis (ICA) model [13] is put forward for MA reduction [14] [15]. It is also used associated with the adaptive filter [16]. In this algorithm, features of different sources in the linear signal will be detected [17], then artefact noise can be reduced [15]. Kalman filtering [18] and singular value decomposition (SVD) [19] are also applied.

As for frequency-based methods, wavelet noise reduction is introduced [20]. Improved techniques include double-tree wavelet transform (DTWT) [21] [22] and ICA-associated WT [23]. Besides, power spectral analysis [24] and sparse spectral analysis [25] [26] also make sense.

In this study, we proposed a robust framework for HR monitoring from PPG signals based on STFT. Traditionally, fast Fourier transform (FFT) was suggested to process the whole raw signal. Then real-time HR cannot be derived using FFT. In this situation, signal segmentation is required, in order to focus a small period of the signal. On the other hand, FFT does not work well for short-time signals, because the resolution is limited. Therefore, FFT is replaced by STFT in our framework [27]. In this paper, a reformative algorithm for HR monitoring using the combination of STFT and spectral analysis is proposed, named as Short-time Fourier Spectral Tracking (SFST). The spectral tracking consists of spectral Detection, verification and predication.

Email address: dxz709@alumni.bham.ac.uk (Teddy Zhao)

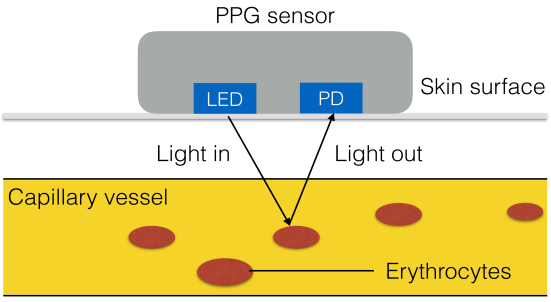

Figure 1: A simplified representation of the PPG signal's acquisition principle. The light sensor is placed on the body surface. Blood flow is monitored by the light sensor, then PPG signals are obtained.

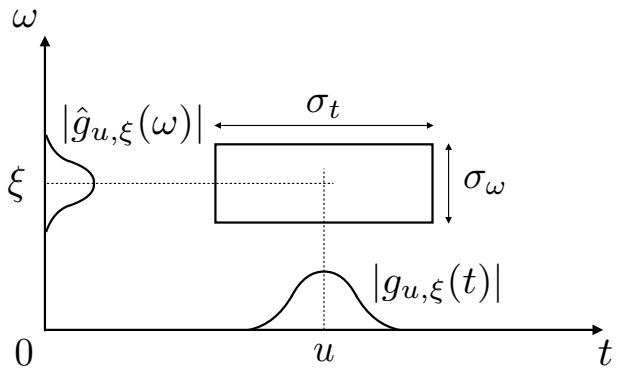

Figure 2: The Heisenberg box of the STFT atom illustrates as the time-frequency plane (t, ω). It can be treated as a rectangle centred at (u, ξ), of size $\sigma_t \times \sigma_\omega$.

2. Background and Motivation

2.1. PPG Principle

The principle of PPG helps with the foundation of the whole framework. The PPG signal is measured from the vascular blood flow measurement sensor. It is originally used to detect arterial oxygen saturation and HR, for cardiac arrhythmias diagnosis [28]. As shown in Figure 1, infrared light is utilised through the skin and into the blood vessels. After that, it is sent back to the detector to measure the blood. The results mainly depend on the oxygen and blood flow to the capillary vessel at every heartbeat. Therefore, the PPG signal can be used to monitor HR. Theoretically, a pure PPG signal contains two parts. The large one is a direct current (DC) signal representing the constant absorption of light when passing through the skin-tissue-bone. The small one indicates the light passing through the arteries aroused by the heartbeat, which is an alternating current (AC) signal.

Practically, the signal monitored from the front-end circuit during physical activities contains several components:

1. The desired vascular volumetric changes caused by blood pulse, which is the desired PPG signal.
2. The ambient noise caused by the ambient light. It can be decreased by shielding the ambient light.
3. The pressure noise caused by breath and muscle movement. It can be removed using an IIR digital filter.
4. The mechanical noise caused by the friction on the skin and the electromagnetic interference (EMI) of the monitor device. It is hard to remove [29].

2.2. Short-Time Fourier Transform

STFT provides a spectrum of high resolution in a short time period, because the fixed-time window $g_{u,\xi}$ causes a fixed time-frequency resolution [30]. This is explained by Heisenberg Inequality. That is, one can only trade time resolution for frequency resolution.

In STFT, the information slice provided by $\langle f, g_{u,\xi} \rangle$ is represented in a time-frequency plane (t, ξ). It can be treated as a rectangle of a position and size depending on the time-frequency spread of $g_{u,\xi}$. $g_{u,\xi}$ is centred at u, for g is even.

Therefore, the time spread around u is denoted by σ_t^2

$$\sigma_t^2 = \int_{\mathbb{R}} (t-u)^2 |g_{u,\xi}|^2 dt = \int_{\mathbb{R}} t^2 |g(t)|^2 dt. \tag{1}$$

Since g is also real and symmetric, the Fourier transform of g is

$$\hat{g}_{u,\xi}(\omega) = \hat{g}(\omega - \xi) e^{-iu(\omega-\xi)}, \tag{2}$$

where the centre frequency is ξ. Thus the frequency spread around ξ, also known as bandwidth, is denoted by σ_ω^2,

$$\begin{aligned} \sigma_\omega^2 &= \frac{1}{2\pi} \int_{\mathbb{R}} (\omega - \xi)^2 |\hat{g}_{u,\xi}(\omega)|^2 d\omega \\ &= \frac{1}{2\pi} \int_{\mathbb{R}} \omega^2 |\hat{g}(\omega)|^2 d\omega. \end{aligned} \tag{3}$$

Two sinusoids will be discriminated only if they are more than σ_t apart [31], [32]. The root-mean-square measure is adopted here. Likewise, two pulses in time can be also discriminated only if they are more than σ_ω apart. Therefore, the resolution in the frequency of the STFT analysis is given by σ_t and σ_ω. The window function translates in time when t increases. In addition, the increase in f causes transposition in frequency with a constant bandwidth. Once a specified window is chosen for the STFT, the time-frequency resolution given by (1) and (3) is fixed over the entire time-frequency plane. In fact, the same window is adopted for all frequencies. The STFT window restricts the temporal and frequency resolution cells [33].

Based on Heisenberg Uncertainty, the temporal variance and the frequency variance of $f \in \mathcal{L}^2(\mathbb{R})$ jointly satisfy

$$\sigma_t^2 \sigma_\omega^2 \geq \frac{1}{4}, \tag{4}$$

which is independent of u and ξ. Thus, $g_{u,\xi}$ corresponds to a Heisenberg box of area $\sigma_t \sigma_\omega$, as shown in Figure 2. The box size is independent of (u, ξ), so a windowed Fourier transform has the same resolution across the time-frequency plane [34].

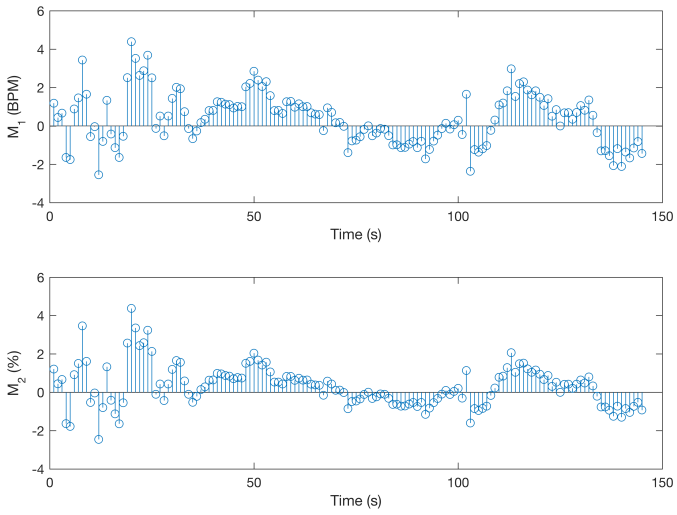

Figure 3: A typical example of true HR via ECG. The two figures show relative percentage and absolute value change of HR during different physical activities, respectively.

By setting a size-fixed window in STFT, the frequency resolution is also fixed. While in WT, the window size is related to the frequency. Therefore, WT does well in time resolution and STFT gains advantages in frequency resolution, in the case of PPG. For the HR-related frequency range, the frequency resolution of STFT is much higher than WT, due to their own properties [35]. Since our aim is to estimate HR by spectral analysis, a higher frequency resolution will be more helpful. Therefore, STFT is chosen instead of WT.

2.3. Heart Rate Observation

The complex noise produces false peaks and makes true peaks vanish, which decreases the accuracy of HR tracking. In this situation, features of true HR shall be observed, in order to formulate the tracking algorithm. Several groups of data were recorded and analysed. M_1 denotes the absolute difference, defined in (5). M_2 denotes the percentage difference, defined in (6). Taking the result shown in Figure 3 as an example, in 0.1s M_1 can only change within [-2.00, 4.00], and M_2 also changes with $[-2.00\%, 4.00\%]$. Then we can infer that HR does not change a lot in a very short time period. To measure and verify the guess, statistic results during different physical activities has been computed. The situations include running, staging and jumping. The result is shown in Table 1. Based on this statistical result, the HR tracking algorithm is proposed.

$$M_1 = \frac{1}{n}\sum_{i=2}^{n} |\mathrm{HR_T}[i] - \mathrm{HR_T}[i-1]| \tag{5}$$

$$M_2 = \frac{1}{n}\sum_{i=2}^{n} \left|\frac{\mathrm{HR_T}[i] - \mathrm{HR_T}[i-1]}{\mathrm{HR_T}[i-1]}\right| \times 100\% \tag{6}$$

Table 1: Statistic result: the absolute difference M_1 and the percentage difference M_2 based on true HR, monitored during different physical activities. The unite of M_1 is BPM.

Dataset	#01	#02	#03	#04	#05	#06
M_1	1.0202	1.2590	1.1974	1.2451	1.1132	0.9527
M_2	0.956%	0.122%	0.992%	1.066%	0.832%	0.832%
Dataset	#07	#08	#09	#10	#11	#12
M_1	0.8053	1.3502	1.0467	0.9159	0.8958	1.1440
M_2	0.648%	1.188%	0.918%	0.6112%	0.620%	0.862%

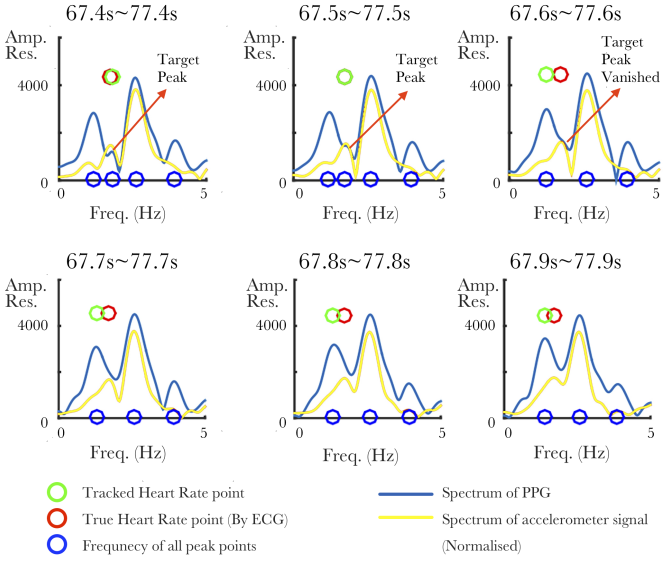

Figure 4: Observation of the frequency spectrum using STFT. The estimated result by spectral peak tracking is right in subplot 1 and 2. However, the peak used in the former two subplots disappears in subplot 3. Another false peak is recognised, which makes the result go wrong from then on.

2.4. Spectrum Observation

The acceleration signal used to carry out spectral subtraction [36]. For validation, we adopted it to our experimental data. A typical result is given by Figure 4. In the first two subplots, the results tracked by the spectral peaks are accurate, according to the true HR via ECG. However, the tracking result from 67.6s to 77.6s is totally wrong, because a false peak is tracked and the target peak vanishes. Even using spectral subtraction, this mistake cannot be corrected. Therefore, improved HR estimation algorithm is required.

3. Method

The flowchart of SFST can be sketched in Figure 5. In the beginning, the signal detected from front-end electric circuit is pre-treated by a baseline filter. Secondly, the signal is segmented with a sliding window and converted into STFT frequency spectrum. In this approach, the spectrum resolution can be improved. After that, HR estimation is carried on via spectral peak tracking. This step contains two parts, verifica-

tion and prediction. In the end, the moving average filter is applied to decrease the influence of values of high variance.

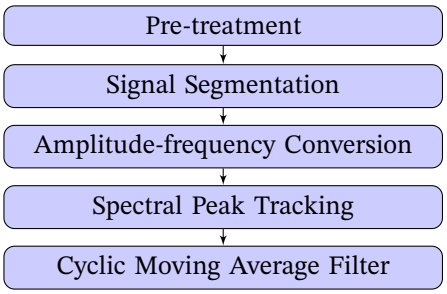

Figure 5: The flowchart of SFST.

3.1. Pre-treatment

The pressure noise performs as the baseline drift. Taking $x_a(t)$ as the raw and analogue PPG signal, obtained from the front-end circuit. x_a is converted into discrete digital data as x_d:

$$x_d \leftarrow x_a. \tag{7}$$

The primary signal is filtered using a zero-phase forward and reverse digital IIR filter [37], whose coefficients are shown in (8). The baseline drift caused by respiration disturbance is then removed. The pre-treatment facilitates signal analysis. The detailed algorithm is given by Algorithm 1.

$$\nu = 2\mu \sin^2(\frac{\pi\mu}{f_s}) - \frac{2\sqrt{\mu}}{1-\mu}\sin(\frac{\pi\mu}{f_s}) + 1 \tag{8}$$

$$x[n] = \frac{\nu}{\nu - 1}(x_d[n] - x_d[n-1]) \tag{9}$$

where

μ the cut-off coefficient;

ν the parameter for the zero-phase forward and reverse digital IIR filter.

μ is often set to 0.3. In some other cases, the value may be various, depending on the intensity of physical activities. The pre-treatment does not change the signal features, but convert it more suitable for peak recognition and HR tracking [37].

Algorithm 1 Pre-Treatment

1: **procedure** PRE-TREATMENT(x_d, μ, f_s) ▷ x_d:the discrete PPG signal, μ: the cut-off coefficient for the IIR filter, f_s: the sampling frequency of x_d.
2: $\nu \leftarrow 2\mu \sin^2(\frac{\pi\mu}{f_s}) - \frac{2\sqrt{\mu}}{1-\mu}\sin(\frac{\pi\mu}{f_s}) + 1$
3: $x \leftarrow x_d$−filtfilt$(1-\nu,[1\ -\nu],x_d)$ ▷ Filter with the zero-phase IIR filter.
4: **return** x
5: **end procedure**

3.2. Signal Segmentation

To estimate HR in real time, a sliding window is in need. Then the signal can be segmented into several periods. The average HR during a time period can be computed. Therefore, a series of results can be estimated, reflecting the real-time HR [38]. The segmentation approach is described by (10) and (11).

$$N = \frac{l_x - T_w f_s}{T_s f_s}, \tag{10}$$

$$y_i[n] = x[T_s f_s(i-1) + n], 1 \le n \le T_w f_s, 1 \le i \le N, \tag{11}$$

where

N the total number of the segmented signals;

l_x the length of x;

T_w the duration of the sliding window;

T_s the step size of the sliding window;

y_i the i-th segmented signal.

3.3. Amplitude-frequency Conversion

To obtain HR from PPG, STFT realises an exact spectral estimation of the input signal spectrum for a short interval, especially for non-stationary signals. The detailed algorithm is given by Algorithm 2. The formula in the discrete time domain can be described as

$$s_i[n] = \sum_{k=1}^{N} y_i[k]\omega[k - l_\omega]e^{-j\frac{2\pi}{N}nk}, n = 1 : N \tag{12}$$

where

s_i the i-th STFT sequence;

ω the window function for STFT.

l_ω the width of the window function for STFT.

Algorithm 2 Short Time Fourier Transform Algorithm

1: **procedure** SHORT TIME FOURIER TRANSFORM($y_i, l_\omega, h, n_f, f_s$) ▷ y_i: the i-th segmented signal; l_ω: length of the function window; h: hop size; n_f: number of FFT points; f_s: sampling frequency.
2: $\omega \leftarrow$hamming(l_ω,'periodic') ▷ Form a periodic function window, Hamming is adopted here.
3: $l_s \leftarrow$ceil$((1 + n_f)/2)$
4: $x_\omega \leftarrow x. * \omega$
5: $s \leftarrow$FFT(x_ω,fix(n_f)) ▷ Use FFT to calculate STFT.
6: $f \leftarrow \frac{0:l_s-1}{n_f} * f_s$
7: **return** $[s, f]$ ▷ s:the STFT sequence, f: the corresponding frequency sequence.
8: **end procedure**

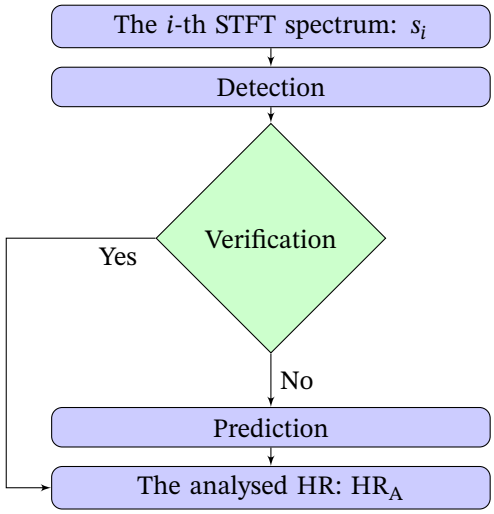

Figure 6: The sub-loop, tracking procedure.

3.4. Spectral Peak Tracking

Although MA has complex effects on PPG signals, their frequency spectrums do not change too much in a short time period. Once the peak representing HR is detected, the change of HR could be tracked. According to the observation on ground truth, HR contains an acceptable divergence in a short time. Therefore, the tracking rules can be proposed, as shown in Figure 6.

3.4.1. Detection

In "Detection", the peak representing HR is detected. For each s_i, all peaks of the STFT spectrum from 0 to 3Hz are found. The corresponding frequency of the peaks are denoted by the sequence f_p.

For the first signal period, the MA is not strong in our experiments, so we treat the HR at this time very close to 60BPM. As the initialisation, the analysed HR is set via

$$\mathrm{HR_A}[i] = 60 \times \arg\min_{f_p} |f_p - 1|. \tag{13}$$

After that, the analysed HR for each loop is detected via

$$\mathrm{HR_A}[i] = 60 \times \arg\min_{f_p} |f_p - \frac{\mathrm{HR_A}[i-1]}{60}|. \tag{14}$$

If no f_p was found, the loop will be skipped, and the $\mathrm{HR_A}[i]$ will be set the same to the former loop.

3.4.2. Verification

"Verification" mainly helps to make sure that the peak detected is not false. Based on the observation of the true HR, its change in a short time is limited. Inspired by this fact, the rule is set by

$$|\frac{\mathrm{HR_A}[i] - \mathrm{HR_A}[i-1]}{\mathrm{HR_A}[i-1]}| < \zeta, \tag{15}$$

where ζ is the parameter making sure that the point verified should not be out of a tolerance. If the limitation cannot be satisfied, the HR shall be predicted instead.

3.4.3. Prediction

"Prediction" deals with the situations that the verification requirement is not satisfied. The prediction rule is based on the change of true HR, given by (16) and (17).

$$\mathrm{HR_A}[i] = \mathrm{HR_A}[i-1] + \frac{1}{l_p}\sum_{j=1}^{l_p} \lambda_j(\mathrm{HR_A}[i-j] - \mathrm{HR_A}[i-j-1]), l_p+1 < i < \tag{16}$$

$$\lambda_j = \begin{cases} 0 & \text{if} \quad |\mathrm{HR_A}[i-j] - \mathrm{HR_A}[i-j-1]| > \kappa \\ 1 & \text{if} \quad |\mathrm{HR_A}[i-j] - \mathrm{HR_A}[i-j-1]| < \kappa \end{cases}, \tag{17}$$

The parameters l_p avoid unexpected iteration caused by one or two detection results. κ and λ help to abandon singular HR values, making the output stable. In this method, most points can be restricted into an acceptable range. The detailed algorithm is given by Algorithm 3.

Algorithm 3 Spectral Peak Tracking

procedure SPECTRAL PEAK TRACKING($f_i, s_i, l_p, \zeta, \kappa$) ▷ For the i-th signal period, import its frequency and STFT amplitude response.
  $[f_p, s_p] \leftarrow$ find peaks of s_i in [0, 3Hz] ▷ Detection
  if $i == 1$ **then**
    $\mathrm{HR_A}[i] \leftarrow 60 \times \arg\min_{f_p} |f_p - 1|$ ▷ Initialisation
  else
    $\mathrm{HR_A}[i] \leftarrow 60 \times \arg\min_{f_p} |f_p - \mathrm{HR_A}[i-1]/60|$
    if $|\frac{\mathrm{HR_A}[i] - \mathrm{HR_A}[i-1]}{\mathrm{HR_A}[i-1]}| > \zeta$ **then** ▷ Verification
      $\lambda_j \leftarrow \mathrm{HR_A}[i-l_p] : \mathrm{HR_A}[i], \kappa$
      $\mathrm{HR_A}[i] \leftarrow \mathrm{HR_A}[i-l_p] : \mathrm{HR_A}[i], l_p, \lambda_j$ ▷ Prediction
    end if
  end if
  return $\mathrm{HR_A}$
end procedure

3.5. Cyclic Moving Average Filter

Due to the complex MA, several values in $\mathrm{HR_A}$ may have unexpected variance. Such values shall be filtered to improve the accuracy. According to the rules adjusted previously, the time spacing in y is $0.1s$. For HR monitoring, it is not necessary to compute HR with such frequency. In this situation, the cyclic moving average filter is introduced to process $\mathrm{HR_A}$ [39].

Considering the analysed result $\mathrm{HR_A}$, it can be segmented into many periods, where each period contains C values.

Then the total number of the periods is N/C. For each period, the mean value is derived. The final estimated HR $\mathrm{HR_E}$ is derived via

$$\mathrm{HR_E}[i] = \frac{1}{C}\sum_{j=1}^{C}\mathrm{HR_A}((i-1)C+j), 1 \le i \le \frac{N}{C}. \quad (18)$$

The corresponding time of $\mathrm{HR_E}[i]$ is derived via

$$t_\mathrm{E}[i] = (i-1)CT_s + \frac{T_w}{2}, 1 \le i \le \frac{N}{C}. \quad (19)$$

The frequency of the final result is derived via

$$f_\mathrm{E} = \frac{1}{CT_s}. \quad (20)$$

In practical work, the output HR at time point t_i is the average value of the previous time period, and the following period will have no effect on this value. That is, once a period is finished, a result is generated as the average value of this period. In this method, the real-time monitoring is realised.

Algorithm 4 Cyclic Moving Average Filter

1: **procedure** CYCLIC MOVING AVERAGE FILTER($\mathrm{HR_A}, N, C, T_s, T_w$)
2: $M(N/C, C) \leftarrow \mathrm{HR_A}$ ▷ Reshape the signal into a matrix.
3: $\mathrm{HR_E}[i] \leftarrow \mathbb{E}[M(i,:)], 1 \le i \le N/C$
4: $t_\mathrm{E}[i] \leftarrow (i-1)CT_s + T_w/2, 1 \le i \le N/C$
5: **return** $\mathrm{HR_E}, t_\mathrm{E}$
6: **end procedure**

4. Experiments

4.1. Implementation

To measure the accuracy of SFST, real-time HR via ECG is used for comparison. Several PPG datasets in [25] have been used to validate the performance of SFST. All datasets were recorded simultaneously from 12 healthy male subjects with age ranging from 18 to 35[1]. In each dataset, the PPG was recorded from the wrist (dorsal) using a pulse oximeter with a green light emitting diode (LED). The wavelength of the green light is 515 nm. The ECG signal was recorded from the chest using wet ECG electrodes. All signals were sent to a nearby computer via Bluetooth, with a sampling frequency of 125 Hz. A signal example is shown in Figure 7, including the raw PPG signal and the ECG signal reference.

The physical activities of subjects are also carefully set. During data recording, the subjects walked or ran on a treadmill with the following speeds in order: the speed of $1 \sim 2$ km/hour for 0.5 minute, the speed of $6 \sim 8$ km/hour for 1 minute, the speed of $12 \sim 15$ km/hour for 1 minute, the speed of $6 \sim 8$ km/hour for 1 minute, the speed of $12 \sim 15$ km/hour for 1 minute, and the speed of $1 \sim 2$ km/hour for 0.5 minute.

[1]For older people and kids, their PPG data may contain unexpected variance for medical reasons.

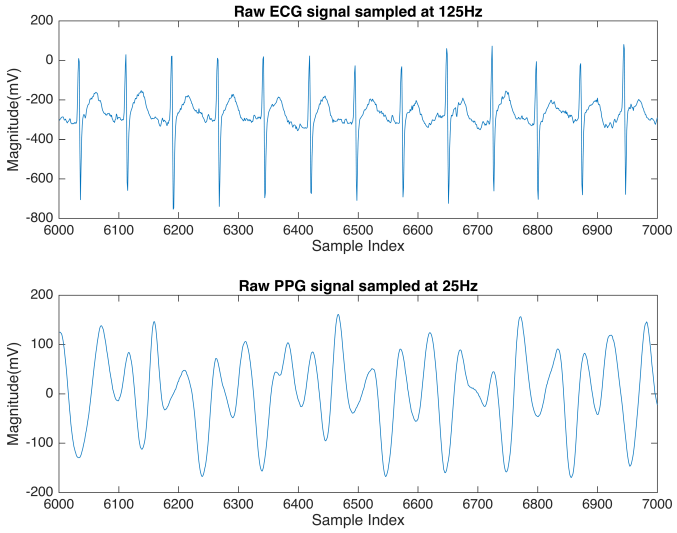

Figure 7: Result of HR tracked using SFST based on dataset 08, randomly selected. As shown in the picture, the estimated HR track is almost of a framework the same with the real-time HR.

4.2. Parameters and Results

To make the result definitely reasonable, a lot of experiments have been conducted in order to increase accuracy. Several parameters of this algorithm have been adjusted by controlling the variables, also observe the input and output of each step or loop. As for the sampling in the first step, the moving windows are controlled by a width of 8s and a step size of 0.1s[2]. To make the output HR refresh with a frequency of 1Hz, the window size in the moving average algorithm is set to be 10. On the other hand, the window function used in STFT is a Hamming window. Hanning, Gaussian and Sine functions are also executable [40] [41].

Figure 8 shows a $\mathrm{HR_E}$ derived from a randomly selected data. Estimated HR is represented with the red dotted line, and the blue line denotes true HR via ECG. As we can see, estimated HR constructs nearly the same framework with real-time HR.

To visualise the result, the STFT frequency spectrogram is computed and shown in Figure 9. Two obvious channels can be found in the figure and one of them represents the real-time change of HR. With the help of the high resolution by STFT, the HR can be located meticulously, making the result proven reasonable.

4.3. Performance Measurement

To measure the performance of HR estimation algorithm, a method proposed in [26] has been adopted here. ε_1 represents the average absolute error (in BPM), and ε_2 represents the average absolute error percentage (both lower is better), defined as

[2]The exact values of window width can be adjusted. A larger window width will enhance the spectrum resolution. The step size is based on the former HR statistic results. A smaller step size will track HR more accurately, but may increase the algorithm complexity at the same time.

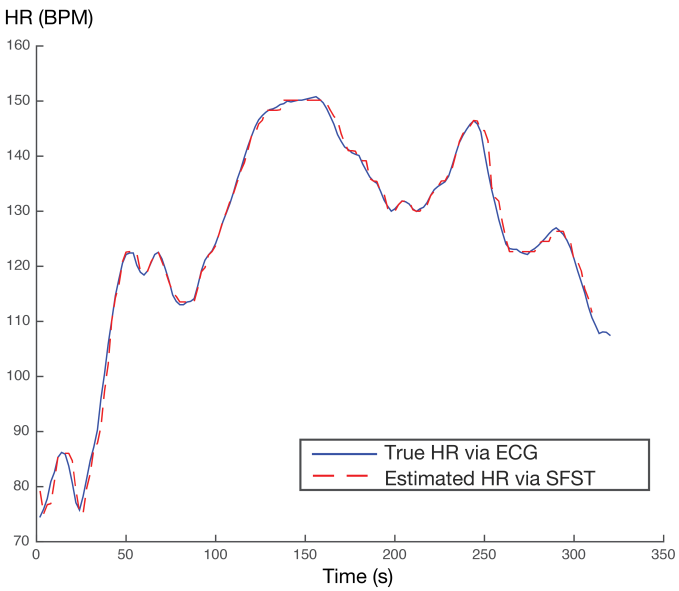

Figure 8: Result of HR tracked using SFST based on dataset 08, randomly selected. As shown in the picture, the estimated HR track is almost of a framework the same with the real-time HR.

Table 2: Comparison between SFST and JOSS in terms of ε on the 12 datasets, AVG denotes average value and SD denotes standard deviation, the unit is BPM.

Dataset	#01	#02	#03	#04	#05	#06	#07
SFST	1.23	1.51	1.19	0.92	0.61	0.78	0.48
JOSS	1.33	1.75	1.47	1.48	0.69	1.32	0.71
Dataset	#08	#09	#10	#11	#12	AVG	SD
SFST	0.49	0.58	3.00	0.73	1.24	1.06	0.69
JOSS	0.56	0.49	3.81	0.78	1.04	1.28	0.89

$$\varepsilon_1 = \frac{1}{n}\sum_{i=1}^{n} |\mathrm{HR_E}(i) - \mathrm{HR_T}(i)|, \tag{21}$$

$$\varepsilon_2 = \frac{1}{n}\sum_{i=1}^{n} \frac{|\mathrm{HR_E}(i) - \mathrm{HR_T}(i)|}{\mathrm{HR_T}(i)}. \tag{22}$$

According to Table II and III, it is obvious that SFST performs better than results in [26] for most datasets. As for statistic results of SFST based on all datasets, the absolute estimation error ε_1 is 1.06 ± 0.69 and the absolute estimation error percentage ε_2 is $0.94\% \pm 0.53\%$. As a comparison, the results of JOSS are 1.28 ± 0.89 and $1.02\% \pm 0.61\%$, respectively. As for cross-correlation between estimated HR by SFST and true HR via ECG based on all 12 datasets, shown in Table IV, the result is 0.9917 ± 0.0141. For 10 out of 12 datasets, the cross-correlation result is higher than 0.99, while the other two sets are also more than 0.95.

The Bland-Altman plot is adopted based on all 12 datasets, given by Figure 10. The limit of agreement between true and estimated HR data is $[-4.3, 3.9]$ BPM, and the coefficient of variation is 1.6%. In addition, a fitting line has been plotted

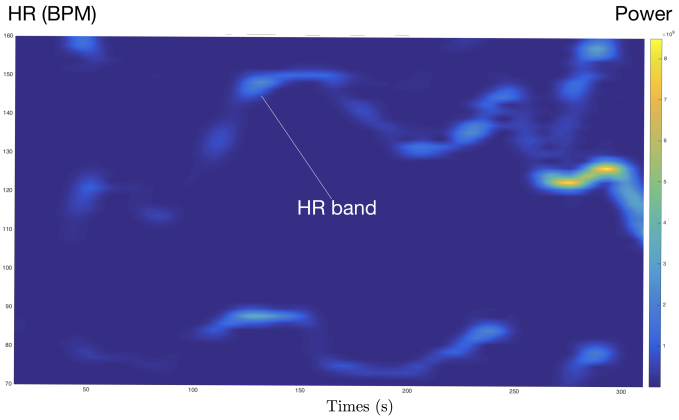

Figure 9: STFT frequency spectrogram of raw PPG signal in dataset 08. The x axis denotes time and HR axis denotes HR. The power denotes the value of amplitude frequency response. A channel in the figure gives the change of HR, referred from real-time HR from ECG signal shown in Figure 8.

Table 3: Comparison between SFST and JOSS in terms of Error2 on the 12 datasets, AVG denotes average value and SD denotes standard deviation, the unit is BPM.

Dataset	#01	#02	#03	#04	#05	#06	#07
SFST	1.11%	1.66%	1.27%	1.41%	0.46%	0.66%	0.38%
JOSS	1.19%	1.66%	1.27%	1.41%	0.51%	1.09%	0.54%
Dataset	#08	#09	#10	#11	#12	AVG	SD
SFST	0.42%	0.50%	1.95%	0.49%	1.01%	0.94%	0.53%
JOSS	0.47%	0.41%	2.43%	0.51%	0.81%	1.02%	0.61%

based on all estimated and true HR data, given by Figure 11 , where the line can be denoted as $y = 1.009x - 1.414$, the sum of squares due to error is 7107, R-square (coefficient of determination) is 0.9927, adjusted R-square (degree-of-freedom adjusted the coefficient of determination) is 0.9927, and root mean squared error is 2.096.

5. Discussion

Adaptive filters and spectral subtraction adopt acceleration signals and help to improve the accuracy of HR estimation, but such work was mainly proposed for scenarios when MA is not strong [26]. Until now, there has been no bibliography that could give a specific description of the relationship between acceleration signals and PPG signals [42]. Nevertheless, some experiments adopting acceleration signals via

Table 4: Cross-Correlation $\rho_{\mathrm{HR_T},\mathrm{HR_E}}$ between true and estimated HR using SFST on the 12 datasets, AVG denotes average value and SD denotes standard deviation

Dataset	#01	#02	#03	#04	#05	#06	#07
$\rho_{\mathrm{HR_T},\mathrm{HR_E}}$	0.9982	0.9950	0.9953	0.9977	0.9977	0.9977	0.9995
Dataset	#08	#09	#10	#11	#12	AVG	SD
$\rho_{\mathrm{HR_T},\mathrm{HR_E}}$	0.9978	0.9993	0.9530	0.9970	0.9728	0.9917	0.0141

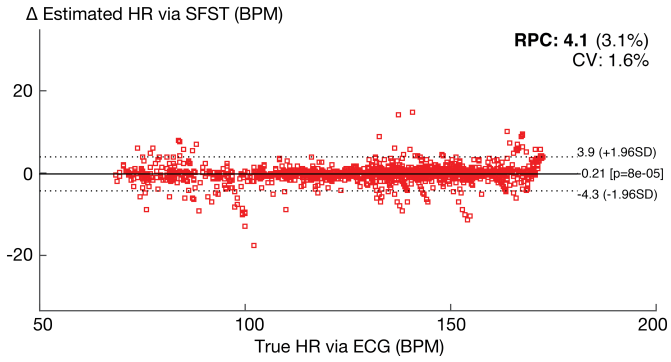

Figure 10: Bland-Altman plot between true and estimated HR, based on all 12 datasets.

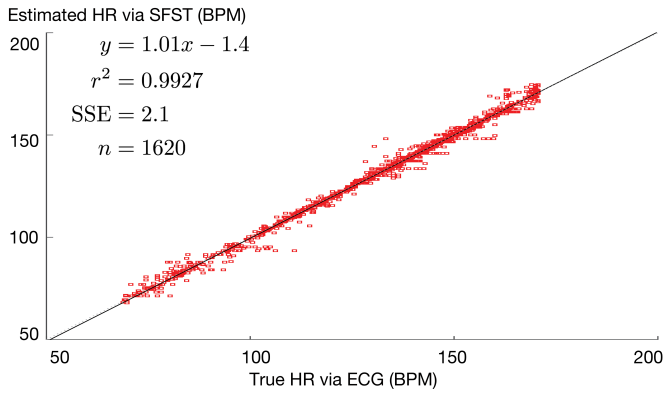

Figure 11: Fitting line between true and estimated HR, based on all 12 datasets.

spectral subtraction are conducted, but their results do not show advantages than SFST's results. In fact, PPG's spectrum does not show connections with acceleration signals based on our research. Therefore, acceleration signals are not listed in our algorithm.

Although Fourier transform or wavelet transform's application in PPG signal processing has been used before [43] [44], the accuracy remains to be improved. In this paper, the proposed solution provides a more general and accurate framework for HR estimation. Despite some methods such as wavelet processing and sparse spectral analysis were adopted before, the proposed method provides a better accuracy, because the change of true HR has been considered and the spectral peak tracking becomes more reasonable. On the other hand, the algorithm may be not feasible for some practical challenges like arrhythmia because its spectral peak tracking is based on true HR, but useful for healthy people for HR monitoring during physical activities.

Compared with methods before, this algorithm has many benefits. Firstly, STFT has the advantage for frequency variation compared with WT [34], helping to improve the tracking accuracy. Secondly, the sampling frequency is set higher than before to make sure HR does not have sudden change. With the help of observation for true HR, the algorithm avoids false tracking between neighbouring loop. Thirdly, moving average filter is added at the end since the sampling frequency is quite high, achieving a continuous result with discontinuity removed. Due to the benefits above, SFST is able to provide higher accuracy.

The Fourier-based algorithm is not the only way to compute frequency spectrum. Other time frequency methods, such as Huang Hilbert Transform and also Gabor transform [45] are known to be more frequencies specific. For the next period, we would like to focus on such methods to process spectrums, in order to develop the algorithm and improve the HR tracking accuracy. On the other hand, the proposed framework relies on the features of health people HR. In the future work, more subjects like older people, women and kids will be tested.

6. Conclusions

In this paper, a robust framework for HR monitoring using PPG signals during physical activities has been proposed, named as SFST. STFT is used to convert frequency spectrum, and peak tracking algorithm is used to carry out spectral analysis in order to estimate HR from PPG signals, without acceleration signals' implementation. With the help of high resolution in low frequency of STFT and second filtering by moving average method, the estimated result is quite reliable, validated by true HR via ECG. Therefore, the proposed robust algorithm is able to derive accurate HR from PPG signals monitored during physical activities. Therefore, SFST is confirmed able to promote the development of wearable devices to monitor HR.

7. Acknowledgments

This research is partially supported by the grants of Southeast University (SEU). The support of experimental equipment is from M-Link, Jiangsu, China. My classmates Wenjie Wang and Shuo Huang provide many useful suggestions for this article.

8. Code Availability

Please contact Teddy Zhao (dxz709@alumni.bham.ac.uk) for requesting code.

Appendix A. Proof of Heisenberg Uncertainty

The following proof is from [46]. Suppose that $\lim_{|t|\to+\infty} \sqrt{t} f(t) = 0$, but the theorem is valid for any $f \in \mathcal{L}^2(\mathbb{R})$.

If the average time and frequency localisation of f is u and ξ, then the average time and frequency location of $e^{-i\xi t} f(t+u)$ is zero. Thus, it is sufficient to prove the theorem for $u = \xi = 0$. Observe that

$$\sigma_t^2 \sigma_\omega^2 = \frac{1}{2\pi ||f||^4} \int_{-\infty}^{+\infty} |tf(t)|^2 dt \int_{-\infty}^{+\infty} |\omega \hat{f}(\omega)|^2 d\omega. \quad \text{(A.1)}$$

Since $i\omega\hat{f}^2(\omega)$ is the Fourier transform of $f'(t)$, according to the Plancherel identity

$$\int_{-\infty}^{+\infty} |f(t)|^2 dt = \frac{1}{2\pi} \int_{-\infty}^{+\infty} |\hat{f}(\omega)|^2 d\omega, \tag{A.2}$$

we have

$$\sigma_t^2 \sigma_\omega^2 = \frac{1}{||f||^4} \int_{-\infty}^{+\infty} |tf(t)|^2 dt \int_{-\infty}^{+\infty} |f'(t)|^2 dt. \tag{A.3}$$

Based on Cauchy–Schwarz inequality

$$|\int_{\mathbb{R}^n} f(x)\overline{g(x)}dx|^2 \leq \int_{\mathbb{R}^n} |f(x)|^2 dx \cdot \int_{\mathbb{R}^n} |g(x)|^2 dx, \tag{A.4}$$

we have

$$\begin{aligned} \sigma_t^2 \sigma_\omega^2 &\geq \frac{1}{||f||^4} [\int_{-\infty}^{+\infty} |tf'(t)f^*(t)|dt]^2 \\ &\geq \frac{1}{||f||^4} [\int_{-\infty}^{+\infty} \frac{t}{2}[f'(t)f^*(t) + f'^*(t)f(t)]dt]^2 \\ &\geq \frac{1}{4||f||^4} [\int_{-\infty}^{+\infty} t(|f(t)|^2)'dt]. \end{aligned} \tag{A.5}$$

Since $\lim_{|t|\to+\infty} \sqrt{t} f(t) = 0$, an integration by parts gives

$$\sigma_t^2 \sigma_\omega^2 \geq \frac{1}{4||f||^4} [\int_{-\infty}^{+\infty} |f(t)|^2 dt]^2 = \frac{1}{4}. \tag{A.6}$$

To obtain an equality, Schwarz's inequality applied to (A.3) must be an equality. This implies that there exists $b \in \mathbb{C}$ such that

$$f'(t) = -2btf(t) \tag{A.7}$$

Thus, there exists $a \in \mathbb{C}$ such that $f(t) = ae^{-bt^2}$. The other steps of the proof are then equalities so that the lower bound is indeed reached. When $u \neq 0$ and $\xi \neq 0$, the corresponding time and frequency translations yield

$$f(t) = ae^{i\xi t - b(t-u)^2}. \tag{A.8}$$

Appendix B. Statistic Approaches

Let $\mathrm{HR_T}$ denote the true HR, $\mathrm{HR_E}$ denote estimated HR by SFST, n denote the total number of all signal points. For Bland-Altman plot[47], the reproducibility coefficient is derived via

$$\mu_D = \mathbb{E}[D] = \frac{1}{n} \sum_{i=1}^{n} D[i], \tag{B.1}$$

$$\mathbb{V}[D] = \mathbb{E}[(D - \mu_D)^2], \tag{B.2}$$

$$\mathrm{RPC} = \sqrt{\mathbb{V}(D)}. \tag{B.3}$$

The coefficient of variation is calculated via

$$\mathrm{CV} = \frac{\mathbb{V}(D)}{\mathbb{E}(D)} \times 100\%, \tag{B.4}$$

where

$$D[i] = 2 \times \frac{\mathrm{HR_T}[i] - \mathrm{HR_E}[i]}{\mathrm{HR_T}[i] + \mathrm{HR_E}[i]}, 1 \leq i \leq n. \tag{B.5}$$

The sum of squared errors of prediction (SSE) between $\mathrm{HR_T}$ and $\mathrm{HR_E}$ is calculated via

$$\mathrm{SSE} = \sum_{i=1}^{n} (\mathrm{HR_T}[i] - \mathrm{HR_E}[i])^2. \tag{B.6}$$

The Pearson's correlation coefficient [48] between $\mathrm{HR_T}$ and $\mathrm{HR_E}$ is calculated via

$$\rho_{\mathrm{HR_T},\mathrm{HR_E}} = \frac{\sum_{i=1}^{n} (\mathrm{HR_T}[i] - \mu_\mathrm{T})(\mathrm{HR_E}[i] - \mu_\mathrm{E})}{\sqrt{\sum_{i=1}^{n} (\mathrm{HR_T}[i] - \mu_\mathrm{T})^2} \sqrt{\sum_{i=1}^{n} (\mathrm{HR_E}[i] - \mu_\mathrm{E})^2}}, \tag{B.7}$$

where

$$\mu_\mathrm{T} = \mathbb{E}[\mathrm{HR_T}], \tag{B.8}$$

$$\mu_\mathrm{E} = \mathbb{E}[\mathrm{HR_E}]. \tag{B.9}$$

References

[1] J. Allen, Photoplethysmography and its application in clinical physiological measurement, Physiological Measurement 28 (3) (2007) 1 – 39.

[2] Y. Mendelson, B. D. Ochs, Noninvasive pulse oximetry utilizing skin reflectance photoplethysmography, IEEE Transactions on Biomedical Engineering 35 (10) (1988) 798 – 805.

[3] T. Tamura, Y. Maeda, M. Sekine, M. Yoshida, Wearable photoplethysmographic sensors - past and present, Electronics 3 (2) (2014) 282 – 302.

[4] K. Nakajima, T. Tamura, H. Miike, Monitoring of heart and respiratory rates by photoplethysmography using a digital filtering technique, Medical Engineering & Physics 18 (5) (1996) 365 – 372.

[5] Adaptive Noise Cancelling: Principles and Applications, Vol. 63(12), IEEE, 1975.

[6] Adaptive Removal of Motion Artifact, Vol. 1, IEEE, 1997.

[7] Low Variance Adaptive Filter for Cancelling Motion Artifact in Wearable Photoplethysmogram Sensor Signals, IEEE, Lyon, 2007.

[8] Reducing Motion Artifact In Wearable Bio-Sensors Using MEMS Accelerometers For Active Noise Cancellation, IEEE, Portland, Oregon, 2005.

[9] Adaptive Reduction of Motion Artefact from Photoplethysmographic Recordings Using a Variable Step-Size LMS Filter, Vol. 2, IEEE, Orlando, Florida, 2002.

[10] Adaptive comb filtering for motion artifact reduction from PPG with a structure of adaptive lattice IIR notch filter, IEEE, Boston, 2011.

[11] M. Ram, K. V. Madhav, E. H. Krishna, N. R. Komalla, K. A. Reddy, A novel approach for motion artifact reduction in ppg signals based on as-lms adaptive filter, IEEE Transactions on Instrumentation and Measurement 61 (5) (2012) 1445 – 1457.

[12] R. Yousefi, M. Nourani, S. Ostadabbas, I. Panahi, A motion-tolerant adaptive algorithm for wearable photoplethysmographic biosensors, IEEE Journal of Biomedical and Health Informatics 18 (2) (2014) 670 – 681.

[13] P. Comon, Independent component analysis, a new concept?, Signal Processing 36 (3) (1994) 287 – 314.

[14] E. Bingham, A. Hyvärinen, A fast fixed-point algorithm for independent component analysis of complex valued signals, International Journal of Neural Systems 10 (1) (2000) 1483 – 1492.

[15] B. S. Kim, S. K. Yoo, Motion artifact reduction in photoplethysmography using independent component analysis, IEEE Transactions on Biomedical Engineering 53 (3) (2006) 566 – 568.

[16] F. Peng, Z. Zhang, X. Gou, H. Liu, W. Wang, Motion artifact removal from photoplethysmographic signals by combining temporally constrained independent component analysis and adaptive filter, Biomedical Engineering Online 13 (1) (2014) 50.
[17] W. Lua, J. Rajapakse, Ica with reference, Neurocomputing 69 (16-18) (2006) 2244 – 2257.
[18] B. Lee, J. Han, H. Baek, J. Shin, K. Park, W. Yi, Improved elimination of motion artifacts from a photoplethysmographic signal using a kalman smoother with simultaneous accelerometry, Physiological Measurement 31 (12) (2010) 1585 – 1603.
[19] Motion Artifact Reduction in Photoplethysmographic Signals using Singular Value Decomposition, IEEE, Warsaw, 2007.
[20] J. E. Fowler, The redundant discrete wavelet transform and additive noise, IEEE Signal Processing Letters 12 (9) (2005) 629 – 632.
[21] I. W. Selesnick, R. G. Baraniuk, N. C. Kingsbury, The dual-tree complex wavelet transform, IEEE Signal Processing Magazine 22 (6) (2005) 123 – 151.
[22] Dual-Tree Complex Wavelet Transform for Motion Artifact Reduction of PPG Signals, IEEE, Budapest, 2012.
[23] M. R. Ram, K. V. Madhav, E. H. Krishna, N. R. Komalla, K. Sivani, K. A. Reddy, Ica-based improved dtcwt technique for ma reduction in ppg signals with restored respiratory information, IEEE Transactions on Instrumentation and Measurement 62 (10) (2013) 2639 – 2651.
[24] M. Nitzan, H. d. Boer, S. Turivnenko, A. Babchenko, D. Sapoznikov, Power spectrum analysis of spontaneous fluctuations in the photoplethysmographic signal, Journal of Basic and Clinical Physiology and Pharmacology 5 (3-4) (1994) 269 – 276.
[25] Z. Zhang, Z. Pi, B. Liu, Troika: A general framework for heart rate monitoring using wrist-type photoplethysmographic signals during intensive physical exercise, IEEE Transactions on Biomedical Engineering 62 (2) (2015) 522 – 531.
[26] Z. Zhang, Photoplethysmography-based heart rate monitoring in physical activities via joint sparse spectrum reconstruction, IEEE Transactions on Biomedical Engineering 62 (2) (2015) 1902 – 1910.
[27] A. N. Akansu, Wavelets and filter banks. a signal processing perspective, IEEE Circuits and Devices Magazine 10 (6) (1994) 14 – 18.
[28] V. F. Blanc, M. Haig, M. Troli, B. Sauvé, Computerized photoplethysmography of the finger, Canadian Journal of Anaesthesia 40 (3) (1993) 271 – 278.
[29] A. Kamal, J. Harness, G. Irving, A. Mearns, Skin photoplethysmography — a review, Computer Methods and Programs in Biomedicine 28 (4) (1989) 257 – 269.
[30] O. Rioul, M. Vetterli, Wavelets and signal processing, IEEE Signal Processing Magazine 8 (4) (1991) 14 – 38.
[31] D. Gabor, Theory of communication. part 1: The analysis of information, Electrical Engineers - Part III: Journal of the Institution of Radio and Communication Engineering 93 (26) (1946) 429 – 441.
[32] C. Torrence, G. Compo, A practical guide to wavelet analysis, Bulletin of the American Meteorological Society 79 (1) (1998) 61 – 78.
[33] M. Portnoff, Time-frequency representation of digital signals and systems based on short-time fourier analysis, IEEE Transactions on Acoustics, Speech and Signal Processing 28 (1) (1980) 55 – 69.
[34] S. Mallat, A Wavelet Tour of Signal Processing, Academic Press, Burlington, 2008.
[35] I. Daubechies, Ten Lectures on Wavelets, Vol. 61, SIAM, 1992.
[36] Estimating Heart Rate using Wrist-Type Photoplethysmography and Acceleration Sensor While Running, IEEE, San Diego, 2012.
[37] S. Mitra, Digital Signal Processing, McGraw-Hill, 2001.
[38] E. Jacobsen, R. Lyons, The sliding dft, IEEE Signal Processing Magazine 20 (2) (2003) 74 – 80.
[39] J. Lee, Motion artifacts reduction from ppg using cyclic moving average filter, Technol Health Care 22 (3) (2014) 409 – 417.
[40] J. B. Allen, Short term spectral analysis, synthesis, and modification by discrete fourier transform, IEEE Transactions on Acoustics, Speech and Signal Processing 25 (3) (1977) 235 – 238.
[41] On the Use of Windows for Harmonic Analysis with the Discrete Fourier Transform, Vol. 66(1), IEEE, 1978.
[42] Detection of Motion Artifacts in Photoplethysmographic Signals based on Time and Period Domain Analysis, IEEE, San Diego, 2012.
[43] Reduction of Motion Artifacts From Photoplethysmographic Recordings using a Wavelet Denoising Approach, IEEE, Kyoto, Japan, 2003.
[44] A Novel Parameter from PPG Dicrotic Notch for Estimation of Systolic Blood Pressure Using Pulse Transit Time, IEEE, Hong Kong, 2008.
[45] R. Bracewell, The Fourier Transform and IIS Applications, Vol. 5, McGraw-Hill, New York, 1965.
[46] H. Weyl, The Theory of Groups and Quantum Mechanics, Dover Publication, New York, 1950.
[47] J. M. Bland, D. Altman, Statistical methods for assessing agreement between two methods of clinical measurement, The lancet 327 (8476) (1986) 307–310.
[48] M. Bland, An Introduction to Medical Statistics, Oxford University Press, New York, 2015.